Gallium-introduced bimetal sites in indium-gallium metal organic framework for efficient electrocatalytic reduction of carbon dioxide into formate

Yang Gao, He Xiao*, Xiaofang Ma, Zhizhu Yue, Chunmei Liu, Man Zhao, Li Zhang, Junming Zhang, Ergui Luo, Tianjun Hu, Baoliang Lv, Jianfeng Jia* and Haishun Wu*
Key Laboratory of Magnetic Molecules & Magnetic Information Materials Ministry of Education, The School of Chemical and Material Science, Shanxi Normal University, Taiyuan 030000, China.
* Corresponding author

E-mail: gaoyang9808@126.com (Y. Gao); xiaohe200808@sxnu.edu.cn (H. Xiao); 1739266658@qq.com (X.F. Ma); yuezhizhu712@163.com (Z.Z. Yue); lcm1553540@163.com (C.M. Liu); zm03030225@sxnu.edu.cn (M. Zhao); zhangli603606@163.com (L. Zhang); zhangjunming@sxnu.edu.cn (J.M. Zhang); luogui1991@sxnu.edu.cn (E.G. Luo); hutj@sxnu.edu.cn (T.J. Hu); lvbl@sxnu.edu.cn (B.L. Lv); jiajf@dns.sxnu.edu.cn (J.F. Jia); wuhs@dns.sxnu.edu.cn (H.S. Wu).

1. Chemicals and materials

Gallium Trinitrate Hydrate (III) ($Ga(NO_3)_3$ xH_2O, 99.99%) and Indium (III) Nitrate Hydrate ($In(NO_3)_3$ xH_2O, 99.9%) were purchased from Adamas-beta. P-Phthalic acid (PTA, 99%) was purchased from Aladdin Scientific Corp. N, N-dimethylformamide (DMF, 99.5%) was purchased from Tianjin Beichen Fangzheng Reagent Factory (China). Anhydrous ethanol (C_2H_5OH, 99.7%) was purchased from Guangfu Technology Co., Ltd. Potassium bicarbonate ($KHCO_3$, 99.5%) was purchased from Tianjin Kemiou Chemical Reagent Co., Ltd (China). Deionized water (DI water, 18.25 MΩ) produced by a UPR-II-100 L water purification system was used in this work. All the chemical reagents are analytical grade and used as received without further purification.

2. The turnover frequency (TOF, s^{-1})

TOF of the electrocatalyst was calculated according to the formula:

$$TOF = \frac{n \div t}{m_{cat} \times \omega \div M_{In}}$$

n: the molar yield of formate, mol.

t: operation time for eCO_2RR, s.

m_{cat}: catalyst mass in the electrode, g.

ω: In loading in the catalyst, wt%

M_{In}: atomic mass of In, 114.82 $g \cdot mol^{-1}$.

3. Supplemental figures and tables

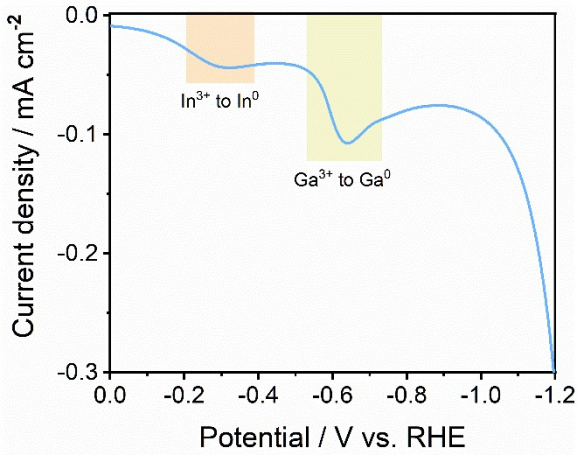

Fig. S1 LSV curve of the solution after ion exchange.

The test utilized a mixture of 0.5 M $KHCO_3$ (25 mL) solution and the solution after ion exchange (5 mL) as the electrolyte. A Pt electrode served as the counter electrode, Ag/AgCl as the reference electrode, and a glassy carbon electrode as the working electrode. The results indicated that the reduction peak of In(III) to In(0) appeared near -0.3 V, while the reduction peak of Ga(III) to Ga(0) appeared near -0.6 V.

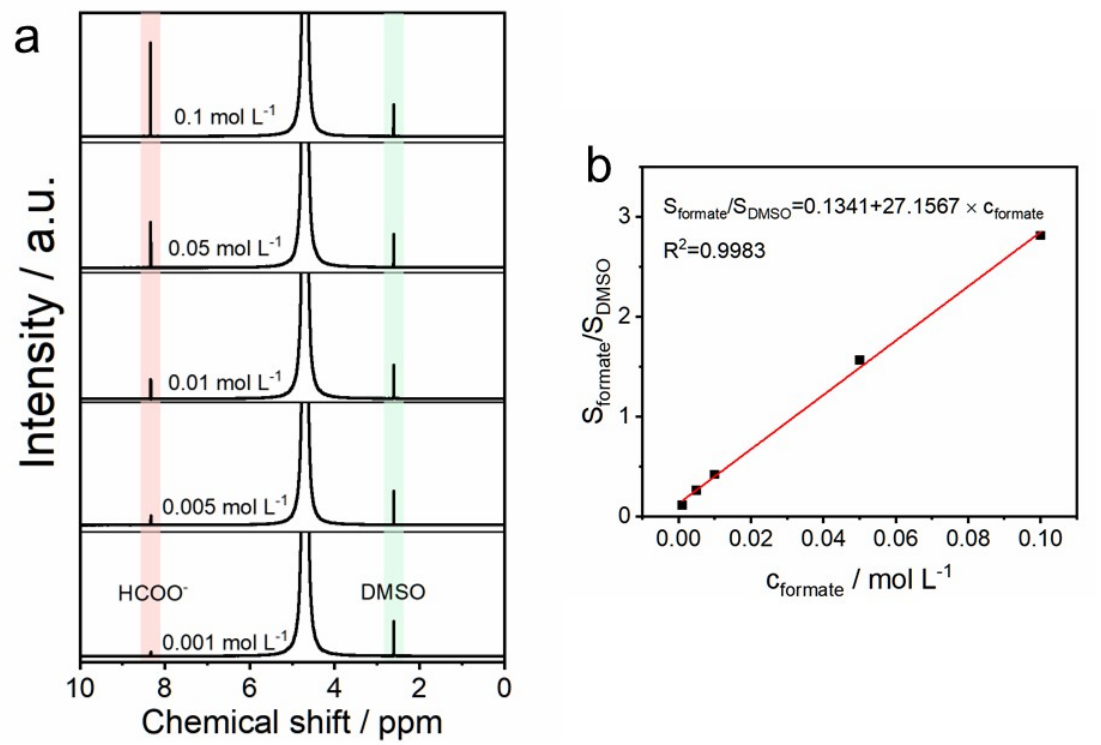

Fig. S2 The standard curve for the formate product.

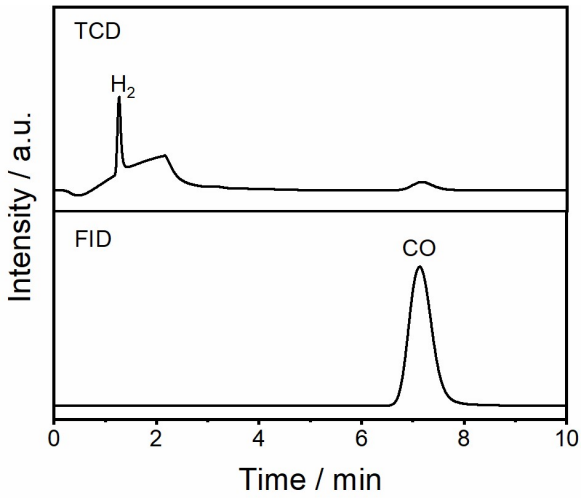

Fig. S3 Gas-chromatography of gas product produced for eCO_2RR.

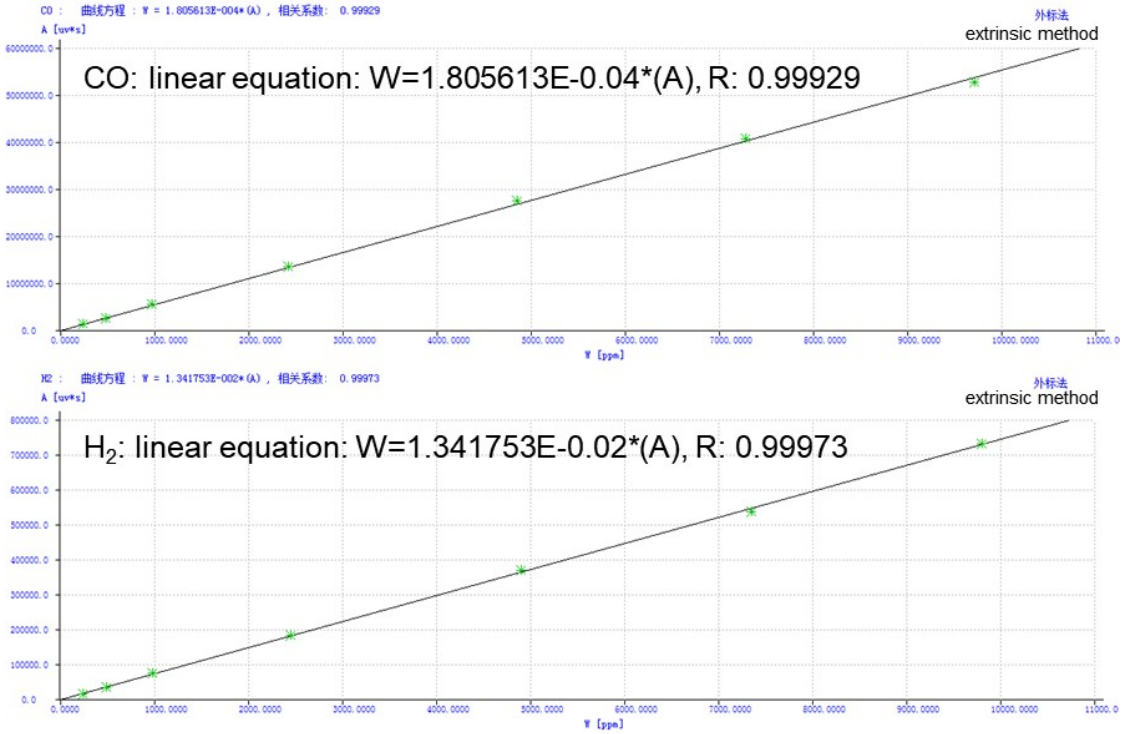

Fig. S4 The standard curves for H_2 and CO product.

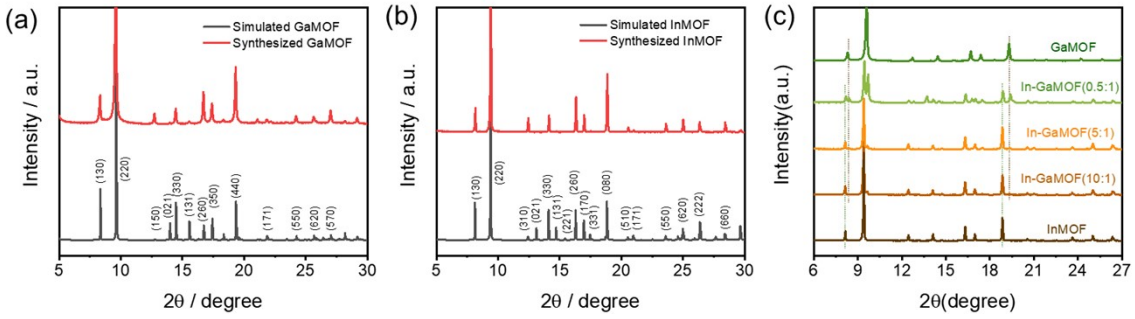

Fig. S5 The simulated XRD of (a) GaMOF and (b) InMOF; (c) the XRD patterns of InGaMOFs with different In/Ga ratios.

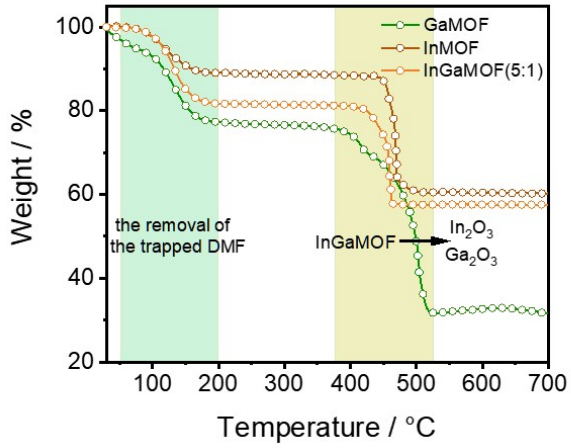

Fig. S6 The TG curves of GaMOF, InMOF, and InGaMOF(5:1).

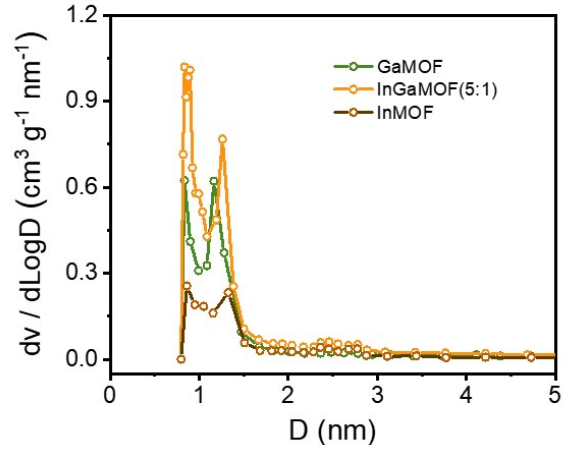

Fig. S7 The pore size distribution calculated by NLDFT method for GaMOF, InMOF, and InGaMOF(5:1).

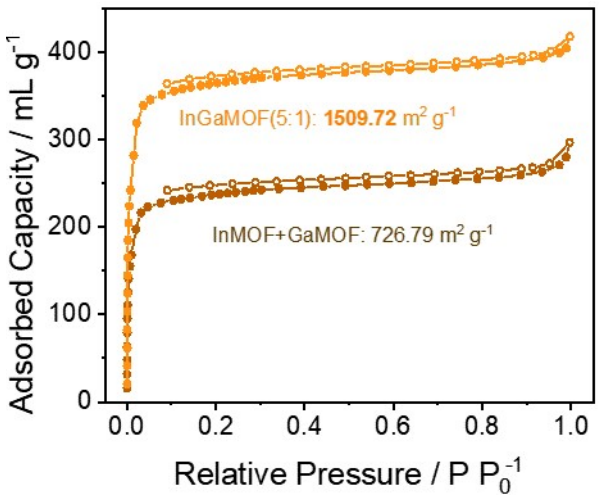

Fig. S8 The N_2 adsorption-desorption isotherms of InGaMOF(5:1) and the physically mixed InMOF+GaMOF.

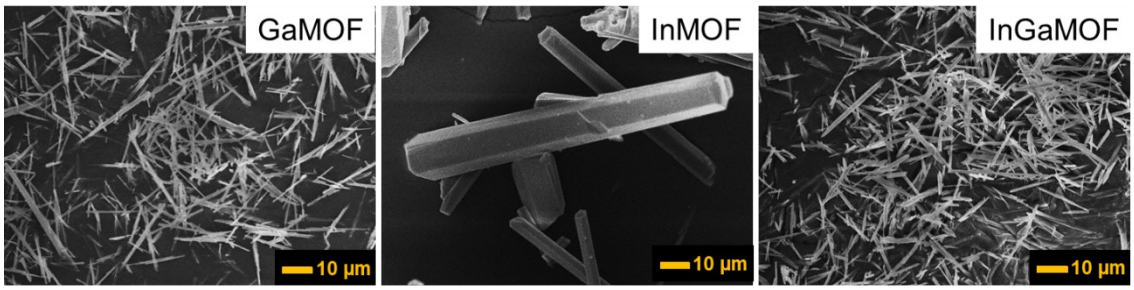

Fig. S9 The SEM image of GaMOF, InMOF, and InGaMOF(5:1).

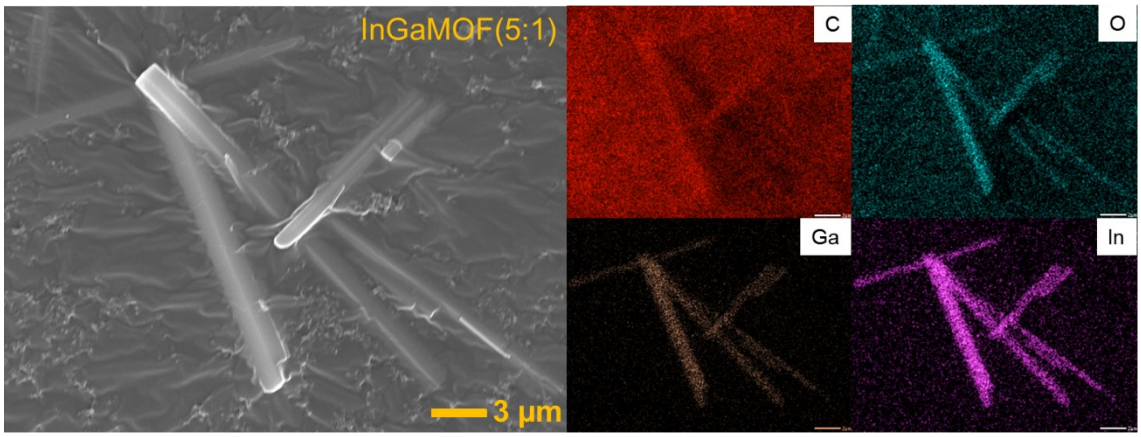

Fig. S10 The SEM and EDX mapping images of InGaMOF(5:1).

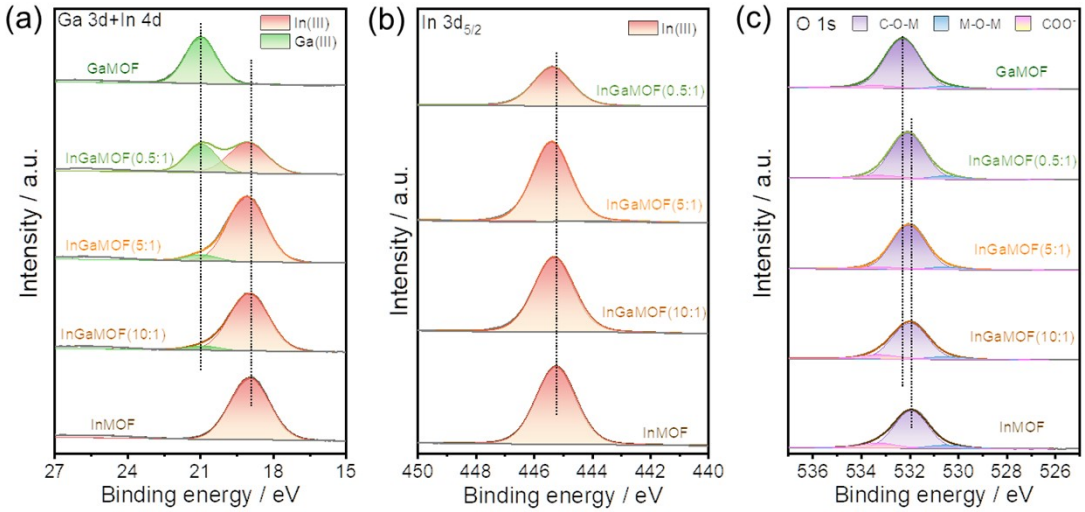

Fig. S11 High resolution XPS spectra for GaMOF, InMOF, and InGaMOFs with different In/Ga ratios.; (a) Ga 3d + In 4d, (b) In 3d, and (c) O 1s.

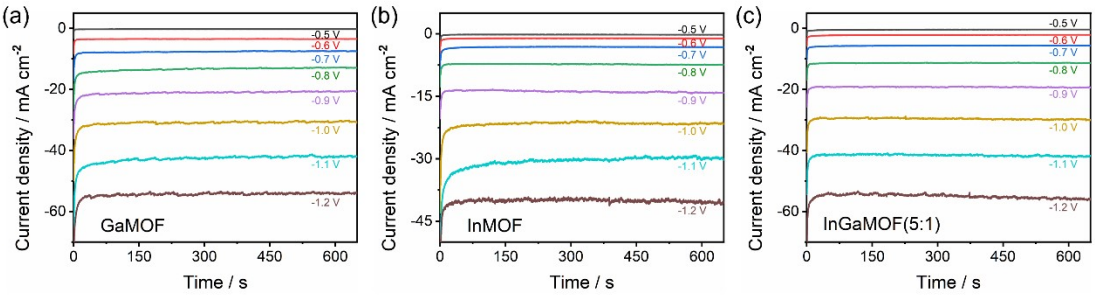

Fig. S12 The i-t curves of GaMOF, InMOF, and InGaMOF(5:1) in CO_2-saturated 0.5 M $KHCO_3$.

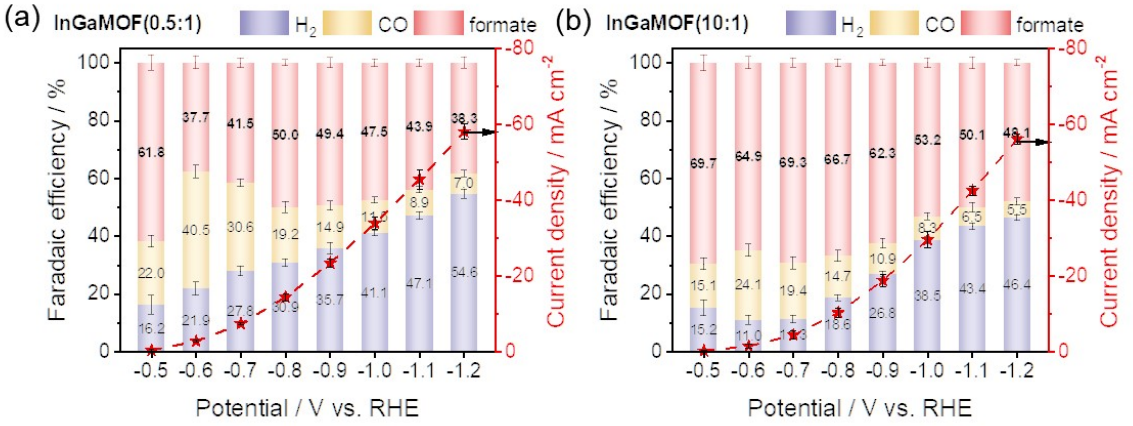

Fig. S13 FEs of product distributions and current density at different applied potentials of InGaMOF(0.5:1) and InGaMOF(10:1).

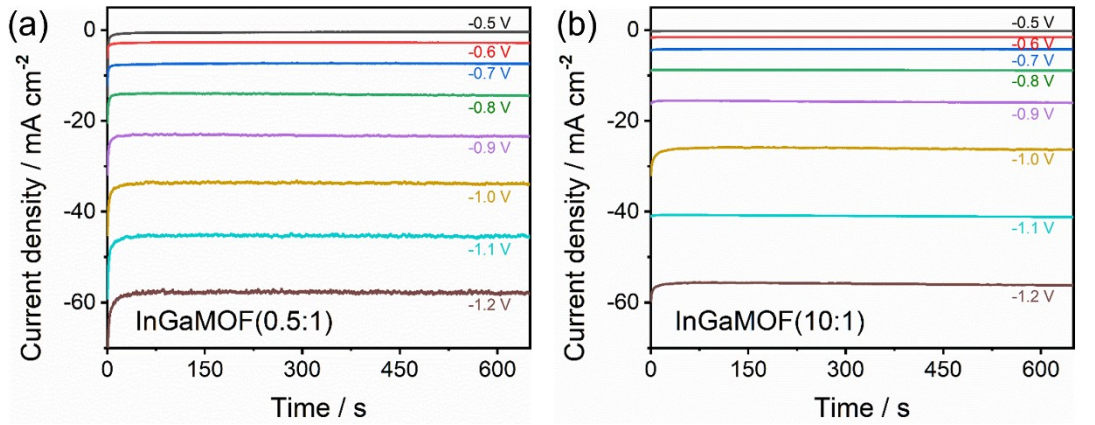

Fig. S14 The i-t curves of InGaMOF(0.5:1)and InGaMOF(10:1) in CO_2-saturated 0.5 M $KHCO_3$.

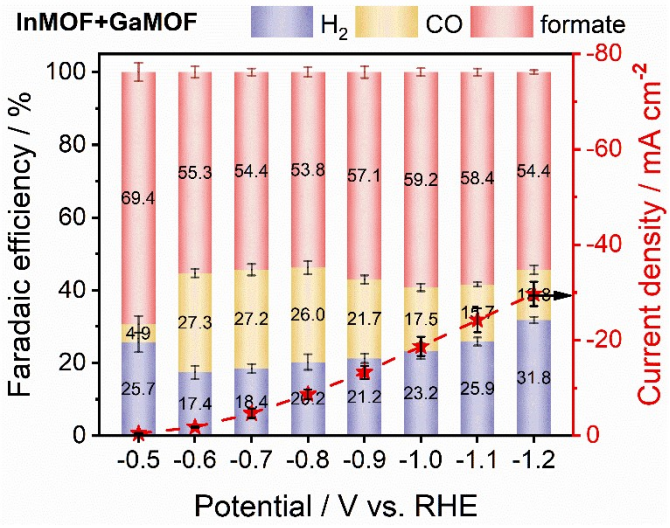

Fig. S15 FEs of product distributions and current density at different applied potentials of physical mixture sample with In-MOF and Ga-MOF.

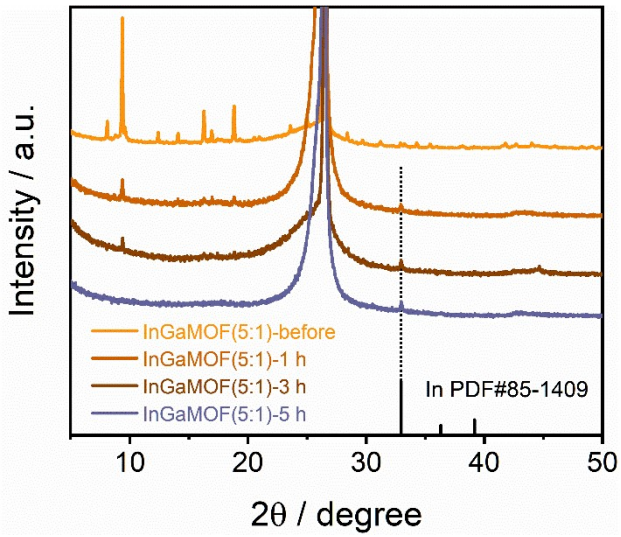

Fig. S16 XRD patterns for InGaMOF(5:1) during the eCO_2RR test.

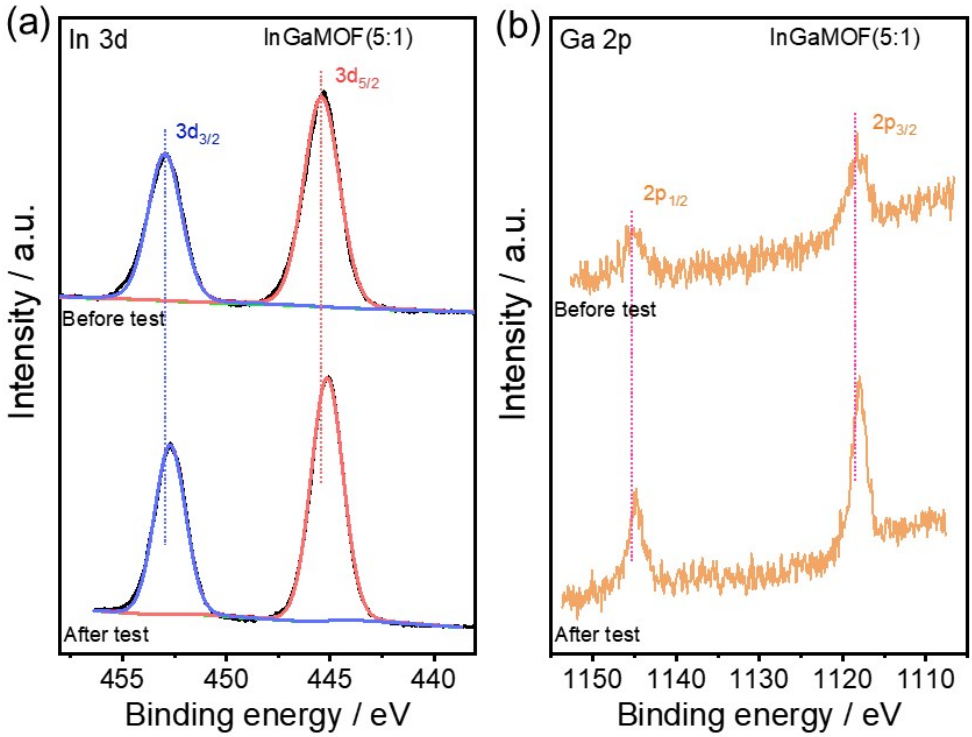

Fig. S17 High resolution XPS spectra for InGaMOF(5:1) after eCO_2RR test.

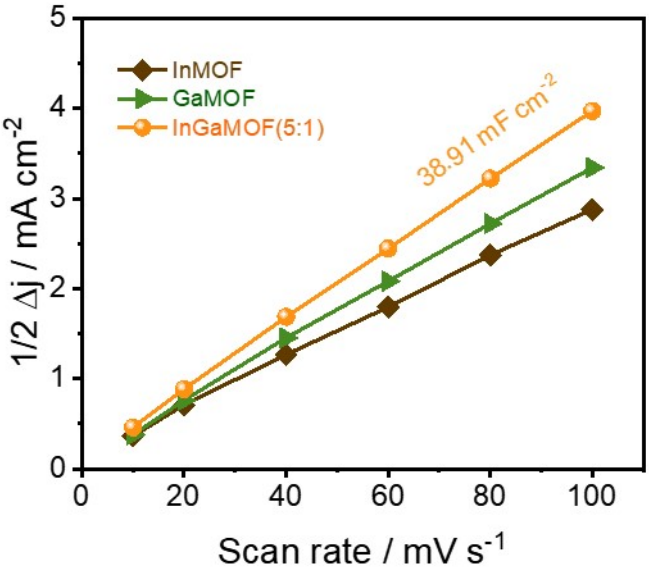

Fig. S18 C_{dl} of GaMOF, InMOF, and InGaMOF(5:1).

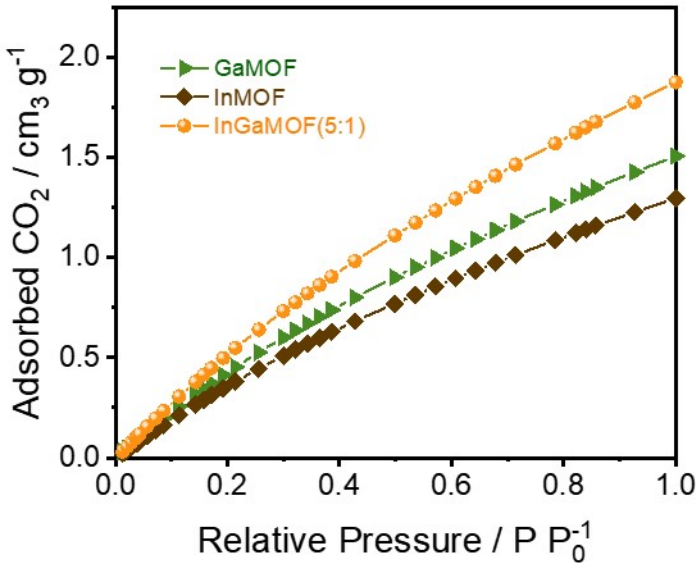

Fig. S19 CO_2 adsorption isotherms of GaMOF, InMOF, and InGaMOF(5:1) at 298 K.

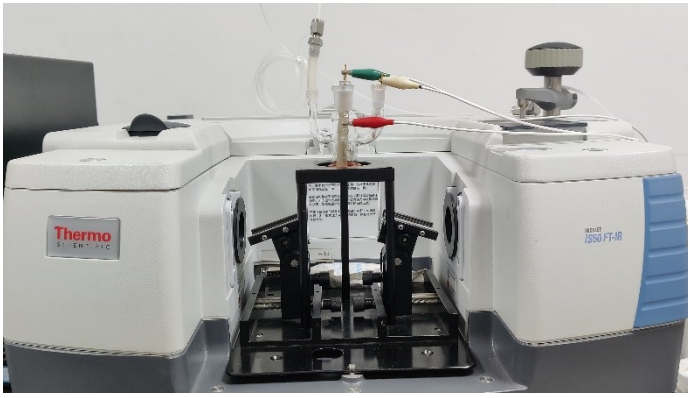

Fig. S20 The *in-situ* FTIR apparatus diagram.

Table S1 Mass fractions of In and Ga in the solution after ion exchange.

Element	Sample volume	Mass fraction
Ga	2 mL	0.002%
In	2 mL	0.0136%

Table S2 The amount of reactant material

	InGaMOF(0.5:1)	InGaMOF(5:1)	InGaMOF(10:1)	InMOF
GaMOF / mg	200	200	200	0
In(III) / mmol	0.5	5	10	3
PTA / mmol	3.6	3.6	3.6	3.6

Table S3 Molar ratios of In and Ga in the InGaMOFs.

	InGaMOF(0.5:1)		InGaMOF(5:1)		InGaMOF(10:1)	
	Feed	ICP-OES	Feed	ICP-OES	Feed	ICP-OES
In/Ga	0.5:1	0.64:1	5:1	6.52:1	10:1	8.21:1

Table S4 The BET values of MOFs.

	InMOF	GaMOF	InGaMOF(5:1)	InMOF+GaMOF
BET Specific Surface Area / $m^2\ g^{-1}$	407.03	801.88	**1509.72**	726.79

The physically mixed 200 mg InMOF and 20 mg GaMOF is noted as InMOF+GaMOF. The In/Ga mole ratios of InGaMOF(5:1) and InMOF+GaMOF are equal.

Table S5 Summary of formate production efficacy of different In-based electrocatalysts reported in literature.

Catalysts	**$FE_{formate}$**	**Potential (V vs.RHE)**	**Ref**
InGaMOF(5:1)	**93.0%**	**-0.5**	**This work**
InO_x-O_v	90.2%	-0.7	[1]
Sn doped In_2O_3	87.0%	-0.8	[2]
InN-C	92.2%	-0.8	[3]
mesoporous-In	90.0%	-1.05	[4]

Cu_xIn_y-OH	85.0%	-1.1	[5]
In-N-C	80.0%	-0.8	[6]
In/ZnO@C	90.0 %	-1.2	[7]
In@InO_x	94.0%	-1.0	[8]
In_2S_3-RGO	91.0%	-1.2	[9]
C@In_2O_3@Bi_{50}	90.0%	-1.36	[10]
F doped $In(OH)_3$	92.5%	-1.2	[11]
In@MWCNTs	90.0%	-1.0	[12]
In_2O_3-O_v	91.2%	-1.27	[13]
InOOH-O_v	92.6%	-0.85	[14]

References

1. J. Zhang, R. Yin, Q. Shao, T. Zhu and X. Huang, *Angew. Chem. Int. Ed.*, 2019, **58**, 5609-5613.
2. H.-R. M. Jhong, U. O. Nwabara, S. Shubert-Zuleta, N. S. Grundish, B. Tandon, L. C. Reimnitz, C. M. Staller, G. K. Ong, C. A. Saez Cabezas, J. B. Goodenough, P. J. A. Kenis and D. J. Milliron, *Chem. Mater.*, 2021, **33**, 7675-7685.
3. P. Hou, X. Wang and P. Kang, *Journal of CO_2 Utilization*, 2021, **45**, 101449-101457.
4. L. Xiao, X. Liu, R. Zhou, T. Zhang, R. Zhou, B. Ouyang, E. Kan, P. J. Cullen, K. Ostrikov and X. Tu, *Energy Convers. Manag.*, 2021, **231**, 113847-113857.
5. Q. Xie, G. O. Larrazábal, M. Ma, I. Chorkendorff, B. Seger and J. Luo, *J. Energy Chem.*, 2021, **63**, 278-284.
6. P. Lu, X. Tan, H. Zhao, Q. Xiang, K. Liu, X. Zhao, X. Yin, X. Li, X. Hai, S. Xi, A. T. S. Wee, S. J. Pennycook, X. Yu, M. Yuan, J. Wu, G. Zhang, S. C. Smith and Z. Yin, *ACS Nano*, 2021, **15**, 5671-5678.
7. X. Teng, Y. Niu, S. Gong, M. Xu, X. Liu, L. Ji and Z. Chen, *Mater. Chem. Front*, 2021, **5**, 6618-6627.
8. Y. Yang, J.-j. Fu, T. Tang, S. Niu, L.-B. Zhang, J.-n. Zhang and J.-S. Hu, *Chinese*

J. Catal., 2022, **43**, 1674-1679.

9. H. Ning, X. Fei, Z. Tan, W. Wang, Z. Yang and M. Wu, *ACS Appl. Nano Mater*, 2022, **5**, 2335-2342.
10. J. Zhai, Y. Hu, M. Su, J. Shi, H. Li, Y. Qin, F. Gao and Q. Lu, *Small*, 2023, **19**, 2206440-2206451.
11. X. An, S. Li, Z. Yang, X. Ma, X. Hao, A. Abudula and G. Guan, *Chem. Eng. J.*, 2023, **455**, 140720-140729.
12. L. Xiao, R. Zhou, T. Zhang, X. Wang, R. Zhou, P. J. Cullen and K. Ostrikov, *Energy Environ. Mater.*, 2023, **0**, e12656.
13. Q. Cheng, M. Huang, L. Xiao, S. Mou, X. Zhao, Y. Xie, G. Jiang, X. Jiang and F. Dong, *ACS Catal.*, 2023, **13**, 4021-4029.
14. F. Ye, S. Zhang, Q. Cheng, Y. Long, D. Liu, R. Paul, Y. Fang, Y. Su, L. Qu, L. Dai and C. Hu, *Nat. Commun.*, 2023, **14**, 1-14.